JMEPEG (2024) 33:10062–10070
https://doi.org/10.1007/s11665-023-08654-2

1059-9495/$19.00

ORIGINAL RESEARCH ARTICLE

High-Cycle Fatigue Properties and Life Prediction of ZK30 Magnesium Alloy at Room and Elevated Temperatures

Zikuan Xu, Lixin Huang, Rui Liu, Hongyi Zhan, Peng Zhang, Chen Dong, Meng Li, Jingru Shen, and Zhefeng Zhang

Submitted: 20 April 2023 / Revised: 24 May 2023 / Accepted: 15 August 2023 / Published online: 25 August 2023

The influences of temperature on the tensile properties and especially high-cycle fatigue behaviors of ZK30 magnesium alloy are investigated. The results show that the fatigue strengths are 87.5, 67.5 and 62.5 MPa at room temperature, 100 and 140 °C, respectively. In order to evaluate the fatigue life, considering the temperature and loading conditions, a comprehensive 2-parameter model based on the dislocation pile-up model has been proposed. This model could predict the fatigue performance in the testing temperature range by using the fatigue performance data at several temperatures. Furthermore, at a constant stress amplitude, a critical testing temperature exists, where an optimal fatigue life can be found for the present magnesium alloy. This model provides a new clue for evaluating the optimum service temperature of the high-temperature materials.

Keywords fatigue life prediction, fatigue strength, high-cycle fatigue, high temperature, magnesium alloy

1. Introduction

With the requirements of energy conservation, emission reduction and the development of vehicle lightweight, the high specific strength of magnesium alloys show great potential to be applied in the automotive industry (Ref 1-4). Among them, the magnesium-zinc-zirconium alloys (ZK series) are currently being considered as one of the best alternatives to aluminum alloys in aerospace and automotive industry, for instance in the manufacture of forged pieces for helicopters or racing engines (Ref 5).

The ZK series alloys are precipitation strengthened by the addition of zinc and grain refined by zirconium (Ref 6, 7). In recent years, the fatigue performance of the material has received attentions (Ref 8, 9). Vasilev et al. (Ref 10) found that the severe plastic deformation could significantly improve the fatigue properties of ZK60. Vinogradov et al. (Ref 11) reported that the integrated extrusion plus equal-channel angular extrusion could also elevate the fatigue performance of ZK60. Li et al. (Ref 12) demonstrated that the addition of the Nd element significantly increased the yield strength, ultimate tensile strength and fatigue strength of a cast Mg-Zn-Zr alloy. In addition, according to the numerous studies on the cyclic plasticity of other series magnesium alloys, the twinning and slipping are very important plastic deformation mechanisms for the magnesium alloy (Ref 13-16). For the high-cycle fatigue behavior of magnesium alloy, He et al. (Ref 17, 18) found that fatigue cracks preferred to initiate and propagate along the slip bands in coarse grains with favorable orientations. Yang et al. reported that micro-cracks were initiated in AZ31B alloy by twinning bands at high stress amplitude in high cycle fatigue (Ref 19); while, Mg-Gd-Y-Zr alloy exhibited a slip-related crack initiation mechanism (Ref 20). In the meantime, Xiong et al. (Ref 21) and Barnett et al. (Ref 22) also claimed that the deformation mechanism underwent a distinctive transition from twinning dominant to slip dominant with decreases in cyclic stress loading.

However, the above studies on the fatigue properties of ZK series alloys were only carried out at room temperature (RT). The high-cycle fatigue performance of ZK30 at elevated temperature is seldom reported. Generally speaking, the high temperature would significantly reduce the high-cycle fatigue strength and fatigue life of the traditional metallic materials (Ref 23, 24). To maximize the potential of the material, the tests were carried out at elevated temperatures as high as possible, which generally exceeded $0.5T_m$ (Melting temperature in Kelvin). There are few reports on the testing temperatures lower than $0.5T_m$ (Ref 25). Nur-Hossain et al. (Ref 25) stated that the effect of the elevated temperature (i.e., 80 °C) on fatigue life of AM60B magnesium alloy is not significant. However, the elevated temperature has obvious effects on both tensile strength and plasticity, and both of them might have influences on the fatigue performance. In addition, the variation of tensile strength and plasticity with temperature might be different. When the testing temperature is lower than $0.5T_m$, the relationship between the temperature and the fatigue performance, including fatigue strength and fatigue life and the corresponding mechanisms are still unclear up to now.

Supplementary Information The online version contains supplementary material available at https://doi.org/10.1007/s11665-023-08654-2.

Zikuan Xu, Rui Liu, Peng Zhang, Chen Dong, and **Zhefeng Zhang**, Shi-changxu Innovation Center for Advanced Materials, Institute of Metal Research, Chinese Academy of Sciences, Shenyang 110016, China; **Lixin Huang**, Binzhou Institute of Technology, Binzhou 256600, China; and Shandong Key Laboratory of Advanced Aluminium Materials and Technology, Binzhou 256600, China; **Hongyi Zhan**, China Science Lab, General Motors Global Research and Development, Shanghai 201206, China; **Meng Li** and **Jingru Shen**, CITIC Dicastal Co., Ltd., Qinhuangdao 066000, China. Contact e-mails: zkxu16s@imr.ac.cn, huanglixin@wqucas.com, pengzhang@imr.ac.cn, and zhfzhang@imr.ac.cn.

In addition, many high-cycle fatigue life prediction models have been proposed so far (Ref 26-30). They can be divided into two categories: (1) the dislocation pile-up model and (2) equivalent initial flaw model, which is applicable to non-defect cracking and defect cracking material, respectively. However, the testing temperature is not considered. Therefore, the models cannot evaluate the fatigue properties at different temperatures.

In this study, the tensile and high-cycle fatigue performance at RT and elevated temperature lower than $0.5T_m$ of the commercial ZK30 alloy is investigated, afterward the corresponding fatigue fracture morphologies were also observed. The different effects of temperature on the fatigue strength and fatigue life were discussed by the dislocation pile-up model. A comprehensive 2-parameter model based on the dislocation pile-up model was proposed. This model could predict the fatigue performance in the testing temperature range by using the fatigue performance data at several temperatures. The aim of this study is to enrich the fundamental understanding about the fatigue performance of ZK30 alloy at RT and elevated temperature, and to supplement experimental data for industrial applications.

2. Material and Methods

The material used in this study is a commercial ZK30 alloy received with forging. Samples for optical microscopy were etched in a solution of acetic picral (6 g picric acid, 100 ml ethanol, 5 ml acetic acid and 10 ml water) after mechanical polishing to reveal grain boundaries. The optical micrographs were taken by OLYMPUS GX71 optical microscopy.

Tensile tests were conducted at RT, 100 and 140 °C in the air at a strain rate of 1×10^{-4} s^{-1} on an electromechanical universal testing machines Instron 5982. To ensure the accuracy of the tests three samples were tested. The configuration of the tensile sample is shown in Fig. 1(a) and the tensile properties of the ZK30 alloy at different temperatures could be seen in Table 1, including tensile modulus E and tensile yield stress σ_{TYS}.

High-cycle fatigue tests were conducted at RT, 100 and 140 °C in the air with the stress ratio $R = -1$ and the frequency of 40 Hz on a hydraulic servo testing system MTS 370.10. The configuration of the fatigue sample and the images of the test platform are shown in Fig. 1(b), (c) and (d). The fatigue tests were not interrupted until the samples broke or the test exceeded 10^7 cycles. All run-out data points were not taken to participate in S-N curve fitting. The staircase method (at least two pairs of data) was employed to calculate the fatigue strength.

Both tensile and high-cycle fatigue tests at elevated temperatures started after 10 mins of heat preservation to ensure a uniform temperature throughout the samples. The fatigue fractures were observed by scanning electron microscopy (SEM) Zeiss sigma 500, and the component analysis was accomplished by the energy dispersive spectroscopy (EDS) on the SEM.

3. Results

3.1 Microstructures

Figure 2(a), (b) and (c) presents the optical micrographs of the ZK30 alloy that show a bimodal grain structure consisting

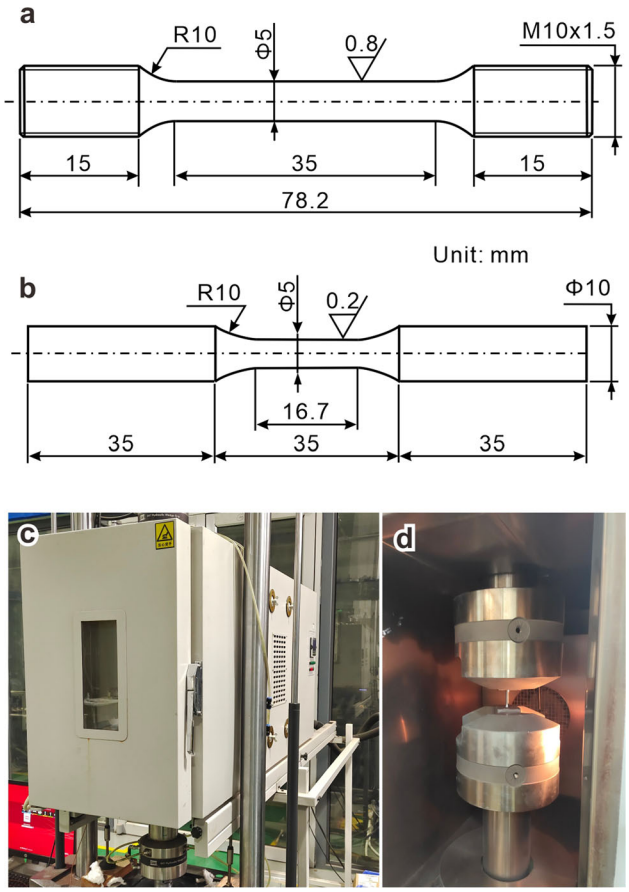

Fig. 1 Samples and the test platform. The configuration of the (a) tensile and (b) fatigue samples. (c) The appearance and (d) inside of the test platform

of ultrafine grains of several microns and coarse grains of about 50 μm in size. This type of microstructure is similar to the results of Oh-Ishi et al. (Ref 31), in which it is called bimodally grained microstructure. It is reported that the Zr-free alloy would show a uniform recrystallized grain structure, while the Zr-containing alloy would show a bimodal grain structure consisting of fine grains of several microns and amorphous coarse grains containing fine precipitates (Ref 31). The microstructure of samples after the fatigue test at 140 °C were observed as shown in Fig. 2(b), and no obvious change in grain size was found. Furthermore, as shown in Fig. 2(d), the precipitates could be identified as Mg(Zn, Zr), which was considered to inhibit dynamic recrystallization, resulting in a partially recrystallized grain structure with bimodal grain distribution (Ref 31-33).

3.2 Fatigue Properties

The relationships between the stress amplitude and the cycles to failure at different temperatures of ZK30 alloy are presented in Fig. 3(a), (b) and (c), in which the red arrows indicate that the samples did not fail up to 10^7 cycles at the specific stress amplitude. The fatigue strengths (σ_{-1}) by staircase method are 87.5, 67.5 and 62.5 MPa at RT, 100 and 140 °C, respectively. It is clear that the increasing temperature has an obvious negative effect on the fatigue strength. For the present magnesium alloy, it shows that the higher the tensile

Table 1 Tensile and fatigue properties at different temperatures

Temperature	E, GPa	σ_{TYS}, MPa	σ_{-1}, MPa	σ_{cr}, MPa	β, MPa
Room temperature	45.2	146 ± 15	87.5	86.6	2728
100 °C	10.9	122 ± 5	67.5	65.9	5057
140 °C	10.7	110 ± 2	62.5	60.7	5577

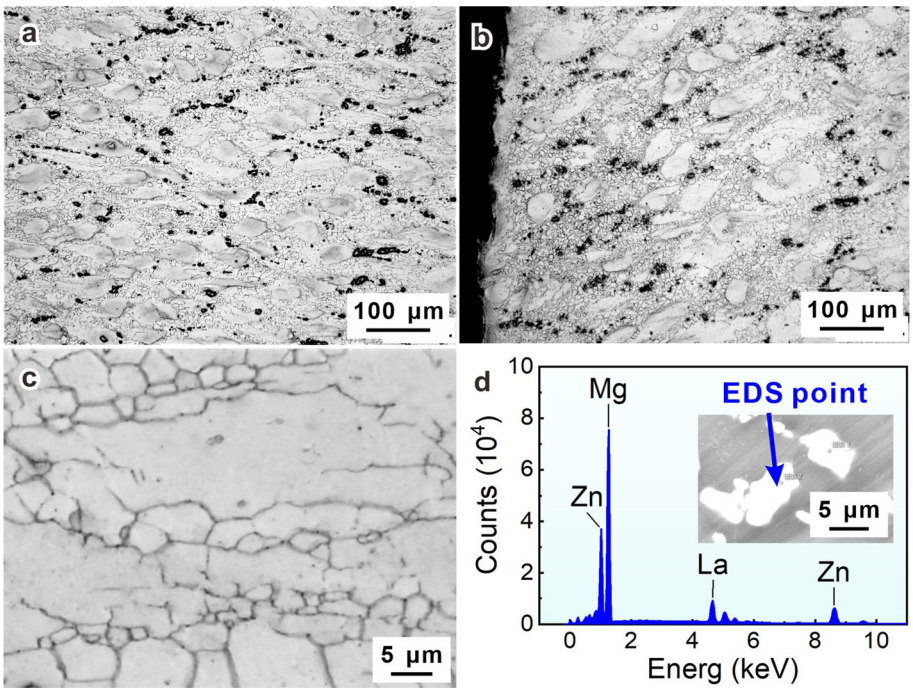

Fig. 2 Optical micrographs of the microstructure of the ZK30 alloy at RT. (a) Before fatigue test. (b) After fatigue test at 140 °C. (c) High magnification image before fatigue test. (d) The EDS results of the marked point in the SEM image of the precipitates

strength is and the lower the tested stress amplitude is, the greater the dispersion of the fatigue life is.

Figure 3(d) shows the comparation of all the data points at three different temperatures. It can be seen that the samples tested at stress amplitude of 105 MPa have almost the same lives for all three temperatures in the present study. Besides, it seems that the testing temperature of 100 and 140 °C only had little effect on fatigue lives compared to RT when the stress amplitude is in the range of 100-110 MPa.

The fatigue strength of ZK30 is not found in the literature. Therefore, several magnesium alloys from other series are list in Table 2 for comparison. The fatigue strength tested at room temperature is between 40 and 150 MPa. The material by squeeze casting has the lowest fatigue strength, and the material by extruded with aging heat treatment has the highest fatigue strength. The material in the present study by rotary swaging exhibits a moderate level of fatigue strength.

The fatigue strength tested at evaluated temperature rarely satisfies $R = -1$ and $N_f = 10^7$, simultaneously, except for AZ61 (Ref 6) and QE22A-T6 (Ref 7). They both have relatively high fatigue strength at evaluated temperature. For AZ61 (Ref 6), the fatigue strength at 150 °C drops down about 50% compared to room temperature. For QE22A-T6, the fatigue strength at 200 °C barely declines 20%. For the present material, the fatigue strength at 140 °C drops down about 29% compared to room temperature, which is at a moderate level.

3.3 Characteristics of Fatigue Damage

To show the typical fatigue fracture morphologies, the sample tested at stress amplitude of 110 MPa were selected for RT, and the different regions of the fatigue fractures surfaces could be observed by SEM, as shown in Fig. 4. The fracture features can be divided into three regions (Ref 34): the region of fatigue crack initiation and early growth, the region of fatigue crack stable propagation, and the final fracture region.

The typical microscopic morphologies of each region at different temperatures are shown in Fig. 5, 6, 7. At all three temperatures, the fatigue crack initiates from the surface of the sample. The SEM images show that there are no defects at the fatigue crack initiation site, such as pores. In the meantime, the EDS results show that there is no obvious intermetallic phase or inclusions at the fatigue crack initiation site. For the propagation region, the fatigue striations can be seen in the microscopic observation. For the final fracture region, the samples at three temperatures all show the characteristics of ductile fracture, and the fracture at 140 °C has the typical dimple morphology.

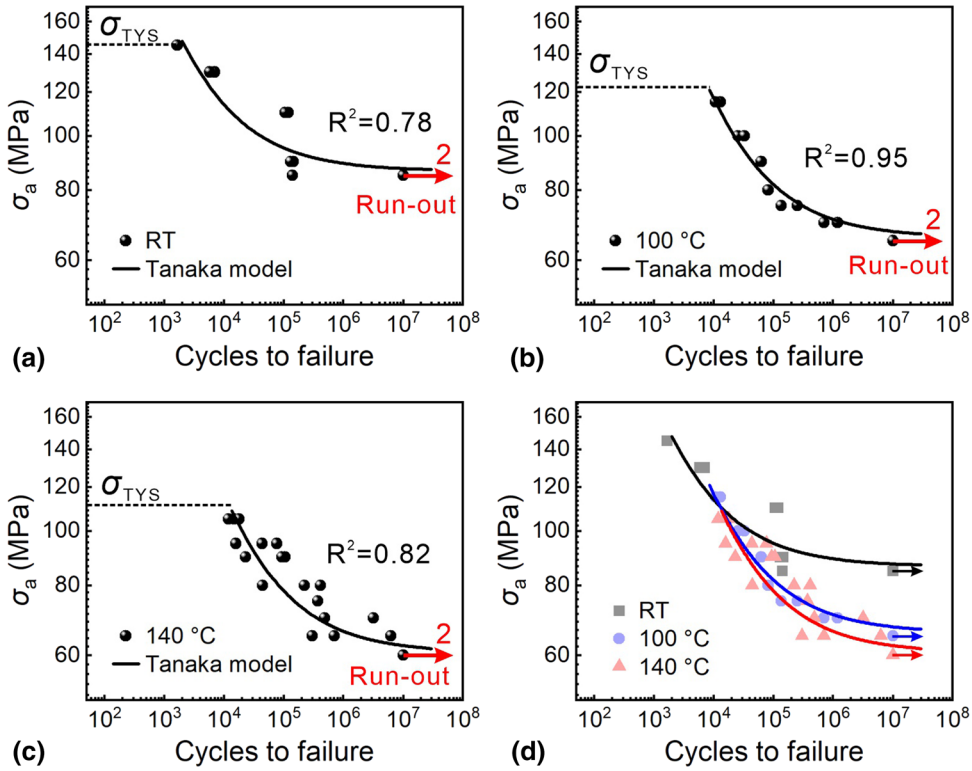

Fig. 3 S-N curves fitted by Tanaka model. (a) RT; (b) 100 °C; (c) 140 °C; (d) comparation of three curves

Table 2 Comparison between the fatigue strength of the present study and the literature

Ref	*T*, °C	Materials	Remark	σ_a, MPa
Ref 43	25	ZK60	As-extruded	140
	25	ZK60-T5		150
Ref 44	25	ZK60	Air	125
Ref 45	25	AZ61A	As-extruded	110
Ref 46	25	AZ31	Squeeze casting	40
	25		Hot-rolled	95
	25		Severely plastically deformed	95
This work	25	ZK30	Rotary swaging	*87.5
	100			*67.5
	140			*62.5
Ref 40	100	WE43-T5	At 10^5 cycles	*150
Ref 47	20	AZ61	55% relative humidity	*157
	20		80% relative humidity	*115
	50		55% relative humidity	*145
	50		80% relative humidity	*115
	150		No relative humidity value	*95
Ref 48	20	QE22A-T6	Sand-cast	*100
	200			*80
	250			*50
Ref 49	150	AM60	At 10^6 cycles, R = 0.1	*31
Ref 50	100	AZ31B	As-extruded	*75
	200			*30
Ref 25	25	AM60B	At 10^6 cycles, R = 0.1	*75
	80			*75
Ref 51	25	Mg12Gd3Y0.5Zr	R = 0.1	74
	100			47
	200			33
	235			25

*Less than three pairs of data points.

4. Discussion

4.1 S-N Curve

According to the Tanaka mode (Ref 35), during the fatigue process, the soft domain in the microstructure would cause strain concentration, which is related to the localization of fatigue damage. The soft domain could be a soft oriented grains in the polycrystalline metals, abnormal large grains produced by partial recrystallization after cold rolling (Ref 36), the soft phase in multiphase metals and the precipitate free zone in the precipitation strengthening material (Ref 37, 38). In addition, the material without metallurgical defects has a fatigue strength at infinite life cycles determined by the critical stress for the initiation of slipping. Furthermore, in the magnesium alloy, the critical stress for the initiation of twinning is equally decisive.

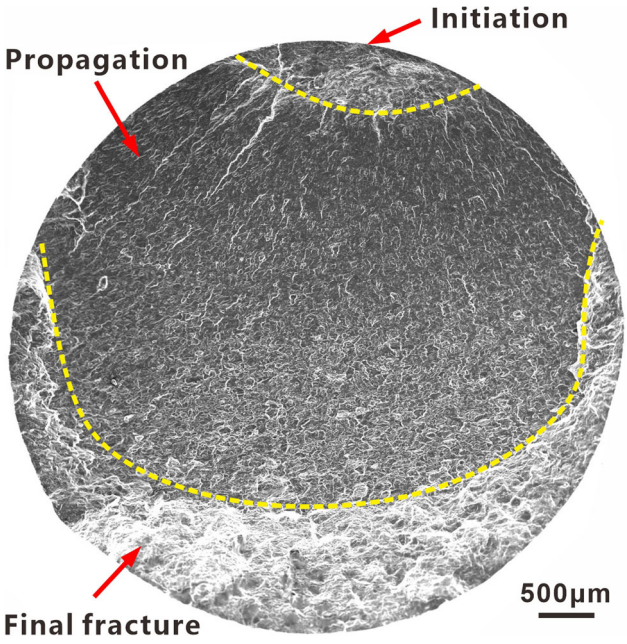

Fig. 4 Typical fatigue fracture of ZK30 at room temperature. Stress amplitude is 110 MPa and fatigue life is 119,384 cycles

Tanaka model can be expressed in the following form (Ref 35):

$$N_i = \frac{AW_S}{(\sigma_a - \sigma_{cr})^2}, \quad \text{(Eq 1)}$$

where N_i is the number of cycles to fatigue crack initiation, A is a constant depending on the material properties, including modulus, the value of W_S is a material parameter referred to fracture energy, σ_a is the stress amplitude, and σ_{cr} is the uniaxial tensile stress corresponding to the critical stress for the initiation of slipping or twinning. Furthermore, it can be written as follows:

$$\sigma_a = \sigma_{cr} + \beta/\sqrt{N_f}, \quad \text{(Eq 2)}$$

where β equals to $\sqrt{AW_S}$. N_i is replaced by N_f since the fatigue crack initiation occupied the most of the total fatigue life (Ref 39). The conditional life fatigue limit σ_{-1} at 10^7 could be used to improve the accuracy of Eq 2. When N_f equals to 10^7, σ_a should equals to σ_{-1}, and σ_{cr} represents the fatigue strength at infinite life. The S-N curves at RT and elevated temperature fitted by Eq 2 are shown in Fig. 3(a), (b), (c) and (d). The values of σ_{cr} and β are listed in Table 1. It could be seen that as the testing temperature increases, β increases. In addition, the σ_{cr} is very close to the conditional life fatigue limit σ_{-1} at 10^7. In addition, for certain data points, such as the sample tested at room temperature under stress amplitude of 110 MPa, the experimental fatigue life is significantly longer than the predicted fatigue life by Tanaka model. After reviewing the original records, it is found that the sample tested at room temperature under stress amplitude of 110 MPa is taken from a wheel hub different from other samples. Along with relatively higher

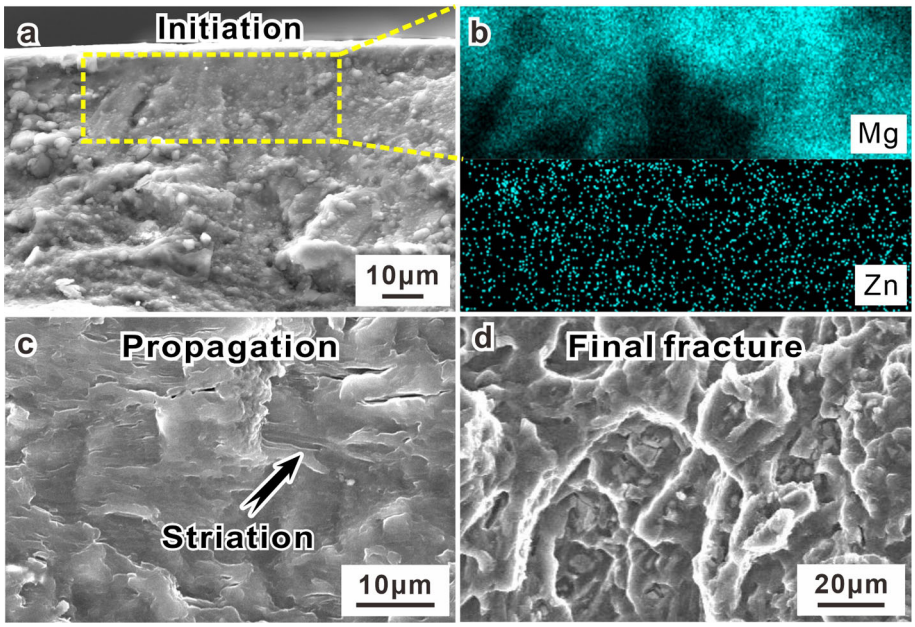

Fig. 5 Typical morphologies of fatigue fracture at room temperature. (a) Initiation region. (b) EDS mapping result in (a). (c) Propagation region. (d) Final fracture region. Stress amplitude is 90 MPa and fatigue life is 146,589 cycles

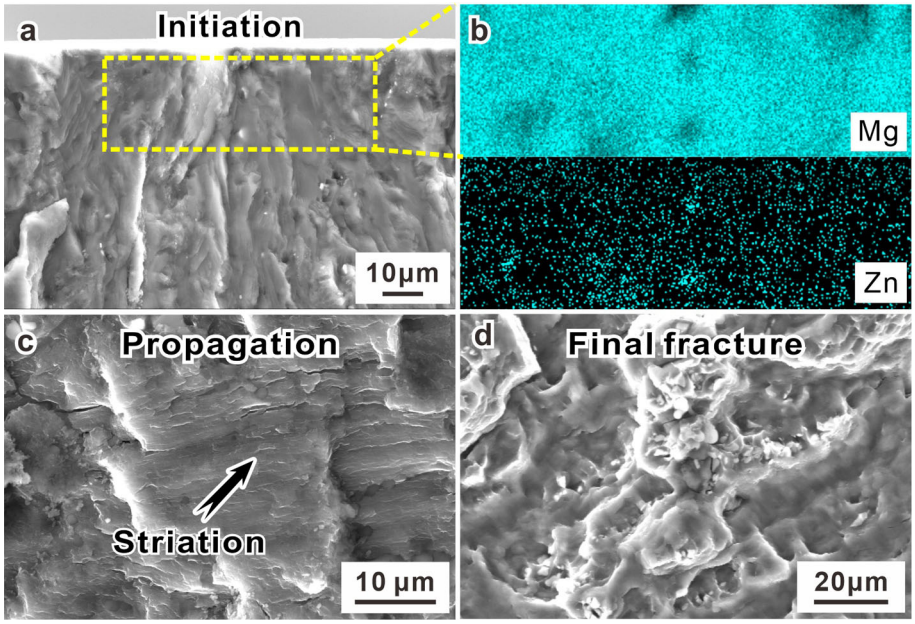

Fig. 6 Typical morphologies of fatigue fracture at 100 °C. (a) Initiation region. (b) EDS mapping result in (a). (c) Propagation region. (d) Final fracture region. Stress amplitude is 70 MPa and fatigue life is 1,196,073 cycles

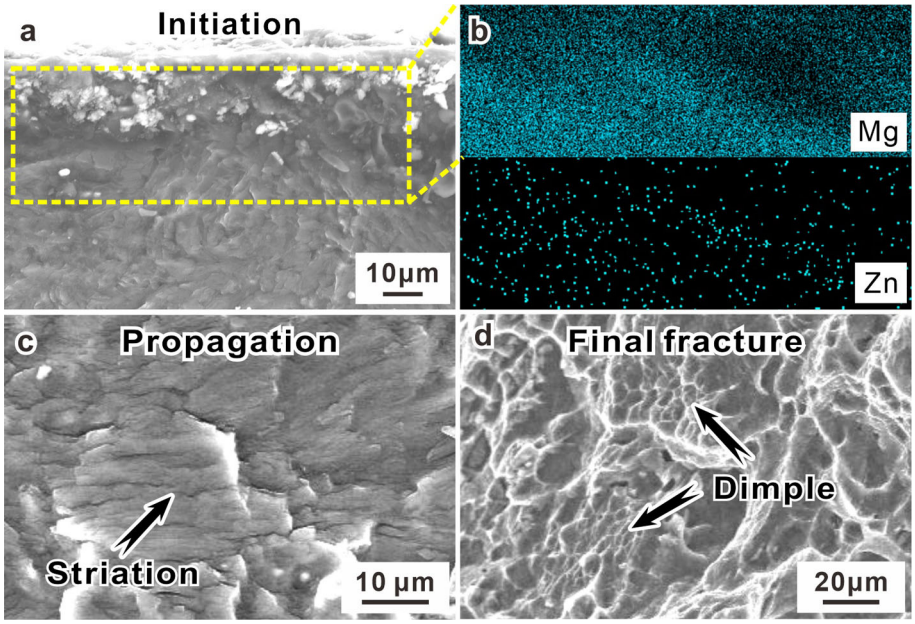

Fig. 7 Typical morphologies of fatigue fracture at 140 °C. (a) Initiation region. (b) EDS mapping result in (a). (c) Propagation region. (d) Final fracture region. Stress amplitude is 65 MPa and fatigue life is 305,401 cycles

tensile strength and lower tested stress amplitude, these might be the reasons that the data have a significant deviation.

4.2 Effect of Temperature on Fatigue Life

It is found that the increasing temperature has an obvious negative effect on the fatigue strength, but has little effect on the fatigue life when the stress amplitude is in the range of 100-110 MPa, which could be seen in Fig. 3(d). According Eq 1, the fatigue life is related to the β and σ_{cr}. Therefore, the effect of temperature on the fatigue life could be attributed to two aspects: β and σ_{cr}.

Firstly, β represents the ability to accommodate fatigue damage. The relationship between β and temperature should be similar to the relationship between the impact energy and temperature, since they both are related to the fracture behavior. It is assumed that β would increase with temperature, but there is a maximum value β_{max} exists, and the closer to the maximum value, the smaller the growth rate is:

$$d\beta = k(\beta_{\max} - \beta)dT. \quad \text{(Eq 3)}$$

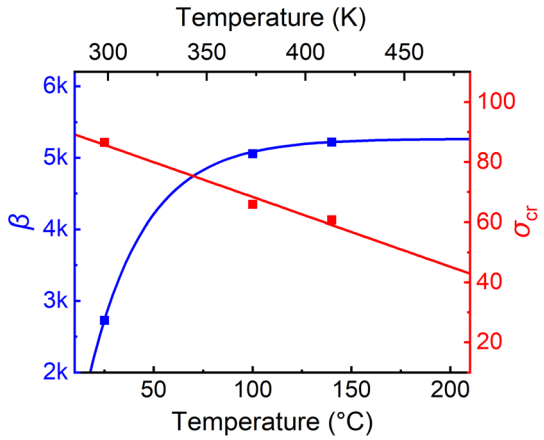

Fig. 8 Relationship between β, σ_{cr} and temperature

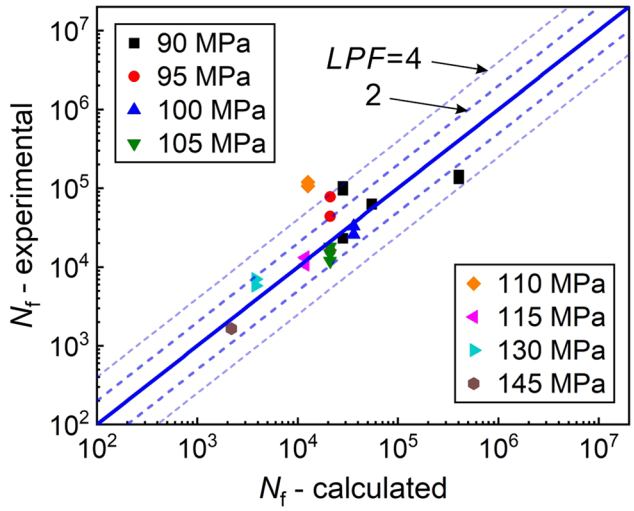

Fig. 9 Prediction of fatigue life by the present model

When the temperature decreases, there is a minimum value β_{min} exists, and the closer to the minimum value, the smaller the growth rate is:

$$d\beta = k(\beta - \beta_{min})dT. \quad \text{(Eq 4)}$$

Therefore, β could not continue to increase when the temperature exceeds a certain value but maintaining a high level. This kind of relationship could be described by:

$$\beta = \beta_{max} - m \cdot e^{-kT} (T \geq T_k), \quad \text{(Eq 5)}$$

$$\beta = \beta_{min} + 1/(n \cdot e^{-kT}) (T < T_k), \quad \text{(Eq 6)}$$

where T_k is similar to the concept of ductile-brittle transition temperature. The unit for the temperature is Kelvin in Eqs 5 and 6. The value of T_k could be obtained by letting β equals to $(\beta_{max} + \beta_{min})/2$. The relationship between β and temperature of the present ZK30 magnesium is shown in Fig. 8. It is clear that the experimental data suit for the model well. In addition, β barely increases when the temperature is higher than 140 °C. The parameters β_{max}, β_{min}, m, k and T_k are constants for a given material and testing condition (e.g., β_{max} = 5264 MPa, β_{min} = 0 MPa, $m = 9.8 \times 10^7$, k = 0.035). The value of T_k could be obtained by letting β equals to $(\beta_{max} + \beta_{min})/2$ then solving Eq 5, and the solution shows that T_k is 298 K (24 °C) for the present material. Then the parameter n could be derived by solving Eq 6 letting β equals to $(\beta_{max} + \beta_{min})/2$, and T_k equals to 298 K, and the solution shows that n is 14.14. Because the testing temperature in the present study is all above the T_k, only Eq 5 is used in Fig. 8.

Secondly, for the fatigue strength (σ_{cr}), it is summarized by Ghorbanpour et al. (Ref 40, 41) that the decline of fatigue strength is associated with the softening of the alloy with increasing the temperature, the underlying softening of the elastic stiffness and thermally activated deformation mechanisms, i.e., easier activation of the crystallographic slip systems. For materials without cracking at micro-scale defect, the fatigue strength is only related to the critical stress for slip initiation of the weakest region in the microstructure (Ref 36, 42). Therefore, high temperature reduces the critical stress for slip initiation and directly leads to the decline of the fatigue strength. The fatigue stress decreases linearly in range of 25-140 °C, as shown in Fig. 8, which can be expressed as follows:

$$\sigma_{cr} = e - f \cdot T. \quad \text{(Eq 7)}$$

The parameters e and f are constants for a given material and testing condition (e.g., e = 91.5 MPa and f = 0.232 °C^{-1} in the present study). Subsequently, the fatigue life at different stress amplitude and temperature could be calculated by substituting Eq 5 and 7 into Eq 2:

$$N_f = \left(\frac{\beta_{max} + m \cdot e^{-kT}}{\sigma_a - (e - f \cdot T)} \right)^2. \quad \text{(Eq 8)}$$

The calculated and experimental results are shown in Fig. 9. The life prediction factor (LPF) is usually used to evaluate the ability of a life prediction method.

$$LPF = \max\left\{ \frac{N_{cal}}{N_{exp}}, \frac{N_{exp}}{N_{cal}} \right\}, \quad \text{(Eq 9)}$$

where N_{cal} and N_{exp} are cycles to failure obtained by the calculation and experiment, respectively. It could be seen that most of the experimental data are within 4 times (LPF = 4) of the predicted life. Furthermore, the fatigue life increases at first and then decreases with temperature increasing at constant stress amplitude (Fig. 10a). Obviously, there is a critical temperature (T_c) at which the fatigue life reaches the maximum value and it can be calculated by:

$$\left. \frac{dN_f}{dT} \right|_{T=T_C} = 0. \quad \text{(Eq 10)}$$

In addition, as the stress amplitude increases, the fatigue life decreases and the T_c increases lightly, as shown in Fig. 10(b). The T_c shows meaning in determining the optimal cooling target temperature to obtain the optimal fatigue life, where the components work at an elevated temperature and cooling is required.

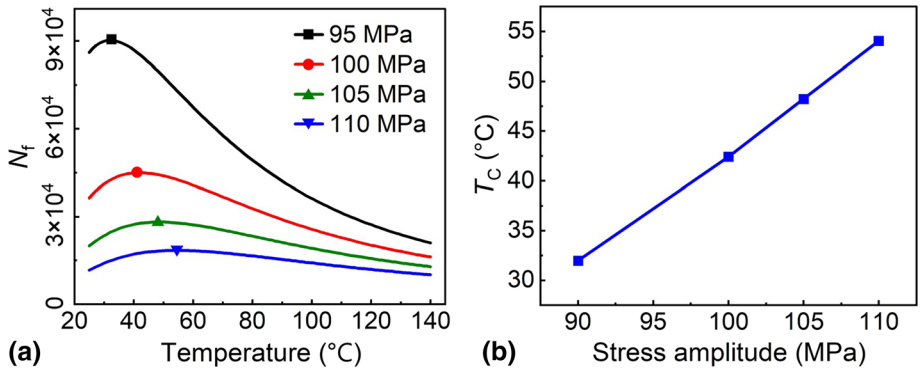

Fig. 10 Prediction of optimal temperature. (a) Relation of N_f-T at constant stress amplitude. (b) Relationship between T_c and stress amplitude

5. Conclusions

The high-cycle fatigue behaviors including crack initiation, fatigue life and fatigue strength of the ZK30 at different temperatures were studied. Based on the experimental results and model analysis, several conclusions can be drawn as follows:

1. The fatigue strengths at 10^7 cycles by staircase method are 87.5, 67.5 and 62.5 MPa at room temperature, 100 and 140 °C, respectively.
2. The fatigue fracture of ZK30 shows similar characteristics under different temperatures: The crack initiation site is free of inclusions and obvious intermetallic phase.
3. The dislocation pile-up model proposed an appropriate form of S-N curve. A 2-parameter model including variable temperature has been proposed. It is realized that a critical fatigue testing temperature (T_c) exists, where the maximum high-cycle fatigue life can be found for the present ZK30 magnesium alloy.

Acknowledgments

This work was financially supported by the National Natural Science Foundation of China (NSFC) under Grant Nos. 52001310 and 52130002, National Science and Technology Major Project of China under Grant No. J2019-VI-0019-0134, IMR Innovation Fund under Grant No. 2022-PY06, the Special Fund Project of High-tech Industrialization Cooperation between Jilin Province and CAS under grant Nos. 2020SYHZ0008 and 2021SYHZ0046, the Open Research Fund from the State Key Laboratory of Rolling and Automation, Northeastern University under grant No. 2021RALKFKT004.

Data Availability

Data will be made available on request.

Conflict of interest

The authors declare no conflict of interest.

References

1. B.L. Mordike and T. Ebert, Magnesium: Properties—Applications—Potential, *Mater. Sci. Eng. A*, 2001, **302**(1), p 37–45
2. M.K. Kulekci, Magnesium and Its Alloys Applications in Automotive Industry, *Int. J. Adv. Manuf. Technol.*, 2008, **39**(9), p 851–865
3. S. Lin, R. Zhu, Y. Wu and Q. Yu, Uniaxial Ratcheting of Extruded Mg-10Gd-3Y Alloy under Stress-Controlled Cyclic Tension, *J. Mater. Eng. Perform.*, 2020, **29**(4), p 2103–2112
4. W. Liu, H. Liu, X. Tong, D. Meng, S. Pang, L. Xiao, L. Jiang and G. Wu, Fracture Behavior of Low-Pressure Sand-Cast Mg-Gd-Y Magnesium Alloy Under Different Types of Loads, *J. Mater. Eng. Perform.*, 2022, **31**(6), p 4483–4494
5. B.L. Mordike and H.E. Friedrich, *Magnesium Technology*, Springer, Berlin, 2006
6. J.D. Robson and C. Paa-Rai, The Interaction of Grain Refinement and Ageing in Magnesium-Zinc-Zirconium (ZK) Alloys, *Acta Mater.*, 2015, **95**, p 10–19
7. D.H. Stjohn, M. Qian, M.A. Easton, P. Cao and Z. Hildebrand, Grain Refinement of Magnesium Alloys, *Metall. Mater. Trans. A*, 2005, **36**(7), p 1669–1679
8. X. Jia, Y.O. Xiang, H.Y. Pei and S. Wei, High-Cycle and Very-High-Cycle Fatigue Behavior of a Stainless Steel for Air-Conditioning Compressor Valve Plates, *Int. J. Struct. Integrity*, 2022, **13**(2), p 185–195
9. X.T. Liu, Q. Wu, S.C. Su and Y.S. Wang, Evaluation and Prediction of Material Fatigue Characteristics Under Impact Loads: Review and Prospects, *Int. J. Struct. Integrity*, 2022, **13**(2), p 251–277
10. E. Vasilev, M. Linderov, D. Nugmanov, O. Sitdikov, M. Markushev and A. Vinogradov, Fatigue Performance of Mg-Zn-Zr Alloy Processed by Hot Severe Plastic Deformation, *Metals*, 2015, **5**(4), p 2316–2327
11. A. Vinogradov, D. Orlov and Y. Estrin, Improvement of Fatigue Strength of a Mg-Zn-Zr Alloy by Integrated Extrusion and Equal-Channel Angular Pressing, *Scr. Mater.*, 2012, **67**(2), p 209–212
12. Z.M. Li, H. Zou, X.J. Feng, J.C. Dai, Z.Q. Xiao and L.M. Peng, Effect of Nd Additions on Fatigue Characteristics of a Cast Mg-Zn-Zr Alloy, *J. Mater. Res.*, 2017, **32**(6), p 1083–1093
13. G.Z. Kang and H. Li, Review on Cyclic Plasticity of Magnesium Alloys: Experiments and Constitutive Models, *Int. J Min. Met. Mater.*, 2021, **28**(4), p 567–589
14. L. Wu, A. Jain, D.W. Brown, G.M. Stoica, S.R. Agnew, B. Clausen, D.E. Fielden and P.K. Liaw, Twinning-Detwinning Behavior During the Strain-Controlled Low-Cycle Fatigue Testing of a Wrought Magnesium Alloy, ZK60A, *Acta Mater.*, 2008, **56**(4), p 688–695
15. Y. Meng, L. Gao, H. Gao and X. Yuan, Effect of Precompression Deformation on the Strain-Controlled Low-Cycle Fatigue Behavior of Extruded AZ31 Magnesium Alloy, *J. Mater. Eng. Perform.*, 2019, **28**(2), p 1007–1018
16. K. Tamada, T. Kakiuchi and Y. Uematsu, Crystallographic Analysis of Fatigue Crack Initiation Behavior in Coarse-Grained Magnesium Alloy Under Tension-Tension Loading Cycles, *J. Mater. Eng. Perform.*, 2017, **26**(7), p 3169–3179

17. C. He, X.H. Shao, S.C. Yuan, L.M. Peng, Y.J. Wu, Q.Y. Wang and Q. Chen, Small Crack Initiation and Early Propagation in an As-Extruded Mg-10Gd-3Y-0.5Zr Alloy in High Cycle Fatigue Regime, *Mater. Sci. Eng. A*, 2019, **744**, p 716–723
18. C. He, Y. Wu, L. Peng, N. Su, Q. Chen, S. Yuan, Y. Liu and Q. Wang, Effect of Microstructure on Small Fatigue Crack Initiation and Early Propagation Behavior in Mg-10Gd-3Y-0.3Zr Alloy, *Int. J. Fatigue*, 2019, **119**, p 311–319
19. F. Yang, S.M. Yin, S.X. Li and Z.F. Zhang, Crack Initiation Mechanism of Extruded AZ31 Magnesium Alloy in the Very High Cycle Fatigue Regime, *Mater. Sci. Eng. A*, 2008, **491**(1–2), p 131–136
20. F. Yang, F. Lv, X.M. Yang, S.X. Li, Z.F. Zhang and Q.D. Wang, Enhanced Very High Cycle Fatigue Performance of Extruded Mg-12Gd-3Y-0.5Zr Magnesium Alloy, *Mater. Sci. Eng. A*, 2011, **528**(6), p 2231–2238
21. Y. Xiong, Q. Yu and Y.Y. Jiang, Multiaxial Fatigue of Extruded AZ31B Magnesium Alloy, *Mater. Sci. Eng. A*, 2012, **546**, p 119–128
22. M.R. Barnett, Z. Keshavarz, A.G. Beer and D. Atwell, Influence of Grain Size on the Compressive Deformation of Wrought Mg–3Al–1Zn, *Acta Mater.*, 2004, **52**(17), p 5093–5103
23. H.Q. Liu, J.C. Pang, M. Wang, S.X. Li and Z.F. Zhang, High-Cycle Fatigue Behavior and Damage Mechanism of Multiphase Al-Si Piston Alloy at Room and Elevated Temperatures, *Adv. Eng. Mater.*, 2018, **20**, p 1700972
24. M.X. Zhang, J.C. Pang, L.J. Meng, S.X. Li, Q.Y. Liu, A.L. Jiang and Z.F. Zhang, Study on High-Cycle Fatigue Fracture Mechanism and Strength Prediction of RuT450, *Mater. Sci. Eng. A*, 2021, **821**, 141599
25. M. Nur-Hossain and F. Taheri, Influence of Elevated Temperature and Stress Ratio on the Fatigue Response of AM60B Magnesium Alloy, *J. Mater. Eng. Perform.*, 2012, **21**(7), p 1395–1404
26. K.S. Chan, A Microstructure-Based Fatigue-Crack-Initiation Model, *Metall. Mater. Trans. A*, 2003, **34**(1), p 43–58
27. Y.B. Xiang, Z.Z. Lu and Y.M. Liu, Crack Growth-Based Fatigue Life Prediction Using an Equivalent Initial Flaw Model. Part I: Uniaxial Loading, *Int. J. Fatigue*, 2010, **32**(2), p 341–349
28. Y.M. Liu and S. Mahadevan, Probabilistic Fatigue Life Prediction Using an Equivalent Initial Flaw Size Distribution, *Int. J. Fatigue*, 2009, **31**(3), p 476–487
29. J.C. Newman, E.P. Phillips and M.H. Swain, Fatigue-Life Prediction Methodology Using Small-Crack Theory, *Int. J. Fatigue*, 1999, **21**(2), p 109–119
30. X.L. Li, W. Li, M.I. Lashari, T. Sakai, P. Wang, Y.C. Zhang, L. Cai, U. Hamid and X.M. Ding, Elevated-Temperature Gigacycle Fatigue Properties of Nickel Based Superalloy: Grain Related Cracking Mechanism and Life Prediction Modelling, *Eng. Fract. Mech.*, 2022, **261**, 108254
31. K. Oh-Ishi, C.L. Mendis, T. Homma, S. Kamado, T. Ohkubo and K. Hono, Bimodally Grained Microstructure Development During Hot Extrusion of Mg-2.4 Zn-0.1 Ag-0.1 Ca-0.16 Zr (at.%) Alloys, *Acta Mater.*, 2009, **57**(18), p 5593–5604
32. J. You, Y.J. Huang, C.M. Liu, H.Y. Zhan, L.X. Huang and G. Zeng, Microstructural Study of a Mg-Zn-Zr Alloy Hot Compressed at a High Strain Rate, *Materials*, 2020, **13**(10), p 2348
33. M. Alvarez-Leal, A. Orozco-Caballero, F. Carreno and O.A. Ruano, Superplasticity in a Commercially Extruded ZK30 Magnesium Alloy, *Mater. Sci. Eng. A*, 2018, **710**, p 240–244
34. T.S. Srivatsan, C. Godbole, T. Quick, M. Paramsothy and M. Gupta, Mechanical Behavior of a Magnesium Alloy Nanocomposite Under Conditions of Static Tension and Dynamic Fatigue, *J. Mater. Eng. Perform.*, 2013, **22**(2), p 439–453
35. K. Tanaka and T. Mura, A Dislocation Model for Fatigue Crack Initiation, *J. Appl. Mech.*, 1981, **48**(1), p 97–103
36. R. Liu, Y.Z. Tian, Z.J. Zhang, P. Zhang and Z.F. Zhang, Fatigue Strength Plateau Induced by Microstructure Inhomogeneity, *Mater. Sci. Eng. A*, 2017, **702**, p 259–264
37. Z.K. Xu, B. Wang, P. Zhang and Z.F. Zhang, A Fast Evaluation Method for Fatigue Strength of Maraging Steel: The Minimum Strength Principle, *Mater. Sci. Eng. A*, 2020, **789**, 139659
38. Z.K. Xu, B. Wang, P. Zhang, Y.K. Zhu, X.G. Wang and Z.F. Zhang, Crack Initiation Mechanism of AISI 4340 Steel for High-Cycle Torsional Fatigue Loading, *Steel Res. Int.*, 2023, **1**, p 2200976
39. X.L. Zheng, On Some Basic Problems of Fatigue Research in Engineering, *Int. J. Fatigue*, 2001, **23**(9), p 751–766
40. S. Ghorbanpour, B.A. Mcwilliams and M. Knezevic, Effects of Environmental Temperature and Sample Pre-straining on High Cycle Fatigue Strength of WE43-T5 Magnesium Alloy, *Int. J. Fatigue*, 2020, **141**, 105903
41. M. Ardeljan, I.J. Beyerlein, B.A. Mcwilliams and M. Knezevic, Strain Rate and Temperature Sensitive Multi-level Crystal Plasticity Model for Large Plastic Deformation Behavior: Application to AZ31 Magnesium Alloy, *Int. J. Plast.*, 2016, **83**, p 90–109
42. H.W. Fu, B. Dönges, U. Krupp, U. Pietsch, C.-P. Fritzen, X.B. Yun and H.-J. Christ, Microcrack Initiation Mechanism of a Duplex Stainless Steel Under Very High Cycle Fatigue Loading Condition: The Significance of Load Partitioning and Micro Residual Stresses, *Acta Mater.*, 2020, **199**, p 278–287
43. W.C. Liu, J. Dong, P. Zhang, Z.Y. Yao, C.Q. Zhai and W.J. Ding, High Cycle Fatigue Behavior of As-Extruded ZK60 Magnesium Alloy, *J. Mater. Sci.*, 2009, **44**(11), p 2916–2924
44. Y.J. Liu, Y. Chen, C. He, F.L. Liu, K. Yang, L. Li, H. Zhang, C. Wang and Q.Y. Wang, Vacuum Retarding and Air Accelerating Effect on the High-Cycle and Very-High-Cycle Fatigue Behavior of a ZK60 Magnesium Alloy, *Mater. Des.*, 2021, **198**, 109310
45. T.S. Shih, W.S. Liu and Y.J. Chen, Fatigue of As-Extruded AZ61A Magnesium Alloy, *Mater. Sci. Eng. A*, 2002, **325**(1–2), p 152–162
46. Z. Zuberova, L. Kunz, T.T. Lamark, Y. Estrin and M. Janecek, Fatigue and Tensile Behavior of Cast, Hot-Rolled, and Severely Plastically Deformed AZ31 Magnesium Alloy, *Metall. Mater. Trans. A*, 2007, **38A**(9), p 1934–1940
47. Z.B. Sajuri, Y. Miyashita and Y. Mutoh, Effects of Humidity and Temperature on the Fatigue Behaviour of an Extruded AZ61 Magnesium Alloy, *Fatigue Fract. Eng. Mater. Struct.*, 2005, **28**(4), p 373–379
48. V.V. Ogarevic and R.I. Stephens, Fatigue of Magnesium Alloys, *Annu. Rev. Mater. Sci.*, 1990, **20**, p 141–177
49. Z. Chen, J. Huang, R.F. Decker, S.E. Lebeau, L.R. Walker, O.B. Cavin, T.R. Watkins and C.J. Boehlert, The Effect of Thermomechanical Processing on the Tensile, Fatigue, and Creep Behavior of Magnesium alloy AM60, *Metall. Mater. Trans. A*, 2011, **42A**(5), p 1386–1399
50. A.H. Jabbari, H. Delavar and M. Sedighi, High Cycle Fatigue Behavior of Magnesium Matrix Nanocomposite at Elevated Temperatures, *Mech. Mater.*, 2020, **142**, 103278
51. X.M. Yang, H.J. Yang, F. Yang, S.M. Yin, W. Wang, S.X. Li and Q.D. Wang, Tensile and Isothermal Fatigue Behaviors of Mg-12Gd-3Y-0.5Zr Alloy at High Temperature, *J. Mater. Sci. Technol.*, 2009, **25**(6), p 731–737